Response of the reconnection electric field and polar cap potential to the IMF and velocity of solar wind

Fukazawa, Keiichiro
Department of Earth and Planetary Sciences, Kyushu University

Aoyama, Tomoharu
Solar-Terrestrial Environment Laboratory, Nagoya University

Ogino, Tatsuki
Solar-Terrestrial Environment Laboratory, Nagoya University

Yumoto, Kiyohumi
Space Environment Research Center, Kyushu University | Department of Earth and Planetary Sciences, Kyushu University

出版情報：Journal of Atmospheric and Solar-Terrestrial Physics. 72 (13), pp.1019-1023, 2010-08. Elsevier
バージョン：

Response of the Reconnection Electric Field and Polar Cap Potential to the IMF and Velocity of Solar Wind

Keiichiro Fukazawa

Department of Earth and Planetary Sciences, Faculty of Sciences Kyushu University

6-10-1 Hakozaki Higashi-ku Fukuoka 812-8581, Japan

fukazawa@geo.kyushu-u.ac.jp

Tel +81-92-641-3131 (ext 8387)

Tomoharu Aoyama

Solar-Terrestrial Environment Laboratory, Nagoya University

Furo-cho, Chikusa-ku, Nagoya 464-8601, Japan

Tatsuki Ogino

Solar-Terrestrial Environment Laboratory, Nagoya University

Furo-cho, Chikusa-ku, Nagoya 464-8601, Japan

Abstract

It is well known that the cross polar cap potential is saturated under a strong interplanetary electric field and is often said to be related to the ionospheric currents. To investigate the other factors influencing this phenomenon, a global magnetohydrodynamics simulation not including the feedback from the ionosphere to the magnetosphere was conducted. The simulation results showed that an increase in the southward IMF causes a smaller increase in the cross polar cap potential than that caused by an increase in the solar wind velocity. This difference was caused by the transportation of reconnected magnetic field lines toward the tail.

Key words

interplanetary electric field, polar cap, MHD simulation

1. Introduction

The polar regions of the ionosphere reflect the dynamics of the global magnetosphere along the magnetic field lines and are important in determining the coupling of the magnetosphere and ionosphere. It is well known that one of these dynamics, the cross polar cap potential, is saturated under a strong interplanetary electric field (IEF), and there have been many suggestions about the mechanism responsible for this saturation (Shepherd, 2007). Sonnerup (1974) and Hill (1975) suggest theoretically that the imbalance between the intensities of interplanetary magnetic field (IMF) and magnetic field of magnetopause decrease the efficiency of dayside merging. However, Nagatsuma (2002) reports that the degree of saturation does not depend on the intensity of dayside reconnection. In the other theory, some suggest that the coupling between ionosphere and magnetosphere is the cause to decrease the polar cap potential (Hill et al., 1976; Fedder and Lyon, 1987; Weimer et al., 1990). However, it has not yet been fully determined as to which mechanism is dominant.

Russell et al. (2001) analyzed several magnetic storm events and reported that the cross polar cap potential increased linearly for an IEF in range of 0–3 mV m^{-1} and began to

50 saturate over 4 mV m^{-1}. MacDugall et al. (2006) recently suggest an enhanced region 2
51 current related to the saturation process of the cross polar cap potential under a strong IMF.
52 Global magnetohydrodynamics (MHD) simulation is often used to examine polar
53 dynamics because the global configuration of the magnetosphere affects the polar regions
54 of the ionosphere. Using global simulation, Siscoe et al. (2002b) found that it was
55 important for the region 1 current to be limited by the solar wind ram pressure for the cross
56 polar cap potential to become saturated. Merkine et al. (2003) compared the results of using
57 two different values of conductivity in their global simulation and concluded that the
58 saturation effect was likely to increase with conductivity. The empirical model of the
59 mechanism responsible for the cross polar cap potential did not adequately describe the
60 saturation of the cross polar cap potential under strong magnetic storms, but Raeder and Lu
61 (2005) indicated that the MHD model described it well. They suggested that shortening the
62 distance of the dayside magnetopause from the Earth caused the cross polar cap potential to
63 saturate. These MHD simulation models include the effects of the feedback from the
64 ionosphere to the magnetosphere; and this effect seems to act as the key factor influencing
65 the polar dynamics.
66 This paper presents the results of our study on the cross polar cap potential based

on the interaction of the solar wind with the Earth's magnetosphere, obtained using a three-dimensional global MHD model. We particularly focus on the effects of magnetic field line deformation on the polar dynamics by not using the ionospheric conductivity in our simulation model and not including feedback from the ionosphere.

2. Simulation model

The basic MHD simulation model has been described in detail by Ogino (1986) and Ogino et al. (1992). We briefly review the model in this section and explain how the present method differs from previous calculations.

We launched a magnetized solar wind with a density of $n_{sw} = 20$ cm^{-3} and a temperature of $T_{sw} = 2 \times 10^5$ K from the upstream boundary of a simulation box and solved the normalized resistive MHD equations as an initial value problem. We used a quarter simulation box with the dimensions $-60\ R_E < X < 30\ R_E$, $0\ R_E < Y < 30\ R_E$, and $0\ R_E < Z < 30\ R_E$ in Cartesian solar magnetospheric coordinates, where R_E is the radius of the Earth ($=6.37 \times 10^6$ m). Thus, the magnetic dipole tilt and IMF B_Y were not included. The number

84 of grid points was (n_X, n_Y, n_Z) = (450, 150, 150) with a uniform grid spacing of 0.2 R_E. The
85 magnetic field (**B**), velocity (**v**), mass density (ρ), and thermal pressure (p) were
86 maintained at solar wind values at the upstream boundary in the simulation. Symmetrical
87 boundary conditions were used at the equator (Z = 0) and meridian plane (Y = 0), while
88 free boundary conditions were used at the top, lateral, and downstream boundaries. All the
89 simulation parameters (**B**, **v**, ρ , p) were fixed for r < 2.5 R_E at the inner magnetosphere
90 boundary. The simulation quantities were connected with the inner boundary through a
91 smooth transition region (2.5 < r < 3 R_E) so that we did not treat the ionosphere as a
92 conductor and have to include the ionospheric feedback effect.
93 We changed two of the solar wind parameters, the velocity of the solar wind and
94 the magnitude of the IMF, to simulate various IEF conditions. The parameters of the solar
95 wind used in the simulation are listed in Tables 1 and 2 along with the magnitude of the
96 IEF calculated from $-V \times B$. Here, the Alfvén Mach number (M_A) is the ratio of the solar
97 wind velocity to the Alfvén velocity. In addition, because it is difficult to achieve a stable
98 simulation with very high speed solar wind, we used solar wind velocities up to 900 km s^{-1}
99 and a constant, high solar wind density of 20 cm^{-3}.
100 The polar cap potential was derived by mapping the results of the global

101 simulation to the ionosphere in a quasi-steady state, as in Park et al. (2006). There are two
102 ways of evaluating the dayside reconnection electric field ($-V \times B$ and ηJ); however, we
103 used the Y-component of $-V \times B$ to compare the upstream electric field in the solar wind
104 with the dayside reconnection electric field. This method is reasonable as these two electric
105 fields connect smoothly in the dayside reconnection region (Walker et al., 1993 and Park et
106 al., 2006).
107
108
109 ## 3. Cross polar cap potential and electric field
110
111 To investigate only the effects of the magnetosphere on the polar dynamics, we
112 carried out an MHD simulation that did not include the ionospheric feedback model, under
113 the conditions listed in Tables 1 and 2. The cross polar cap potential and the dayside
114 reconnection electric field at the subsolar point obtained from the simulation are plotted **Figure 1**
115 against increasing solar wind velocity and IMF B_Z magnitude in Figs. 1 and 2, respectively.
116 The Y-component of the dayside reconnection electric field (RX E_Y) was measured as the
117 maximum E_Y in the immediate vicinity of the reconnection site on the Sun-Earth line. In

both figures, the horizontal axis represents IEF E_Y; the left vertical axis, the potential; and the right vertical axis, the electric field. The dashed line is an approximation of the plot. The range of IEF E_Y is shorter in Fig. 1 than in Fig. 2, as seen in Tables 1 and 2. In these simulation we change the solar wind parameters intermittently as Table 1 and 2, do not change continuously thus the IEF E_Y and potential in Figs 1and 2 seem to be scattered. In addition, dayside reconnection site moves temporally and spatially when the solar wind is changed thus it is difficult to determine when and where reconnection occurs. In this study the IEF E_Y and potential are represented on the Sun-Earth line after 40 minutes passed.

Fig. 1 shows that the cross polar cap potential (black circles) increases linearly with solar wind velocity. In the range of IEF E_Y values between 3×10^{-3} and 4.5×10^{-3} V m^{-1}, the magnitude of the cross cap potential in Fig. 1 (varying solar wind velocity) is almost twice that in Fig. 2 (varying IMF magnitude). In Fig. 1, the approximated line, which has a gradient of about 70.0, can be drawn to pass through the origin and corresponds well with the simulation results. In this case, RX E_Y is enhanced to values greater than the input E_Y (IEF E_Y) at solar wind velocities greater than 600 km s^{-1}. An increase in the solar wind velocity causes an increase in the plasma temperature of the magnetosphere due to shock heating. And this leads to a high plasma velocity in the

Figure 2

magnetosphere, which, in turn, leads to high RX E_Y. In addition, high-speed solar winds (which imply a high dynamic pressure) cause variations in the configuration of the magnetopause and shift the site of reconnection away from the subsolar point. This then would affect the variation in RX E_Y on the Sun-Earth line, which does not exhibit a monotonic increase. However, it is fair to say that the overall variational trend is clearly growth.

In contrast, Fig. 2 indicates that the cross polar cap potential does not exhibit a similar increase with IEF E_Y. The approximated line has gradient of about 8.9 and cannot pass through the origin. The trend of the potential is similar to that seen in Fig. 2 in Siscoe et al. (2002b); however, the range of potentials is different, and in our simulation, the potential is not completely saturated. The dependency of the cross polar cap potential on M_A is similar to that seen in the results of Ridley (2005). He concluded that the cross polar cap potential is saturated at small M_A. The black triangles in Fig. 2 plot RX E_Y, which also does not exhibit a significant increase. RX E_Y increases gradually until an IEF E_Y of 9×10^{-3} V m^{-1} and then decreases slightly until an IEF E_Y of 15×10^{-3} V m^{-1}. RX E_Y becomes smaller than the input E_Y when increasing the magnitude of the southward IMF. Although the ranges of IEF E_Y used in Figs. 1 and 2 are different, it is quite apparent that the

152 behaviors of the cross polar cap potential and RX E_Y are unlike.

153 As the potential and electric field are generally related by $\mathbf{E} = -\nabla\phi$, the potential
154 is not proportional to the electric field. In other words, the scale of the potential is
155 dependent on both the strength and extent of the electric field. The dayside reconnection
156 electric field drives magnetospheric convection and the solar wind then draws the edges of
157 the reconnected magnetic field lines, thereby strengthening the convection. Here, the effect
158 of the convection electric field on the cross polar cap potential is much stronger than that of
159 the reconnection electric field. Thus, the behavior of RX E_Y is not directly linked to the
160 behavior of the cross polar cap potential. The relation between RX E_Y and the cross polar
161 cap potential is discussed in the next section along with the saturation mechanism.

162 Our simulation results revealed that the cross polar cap potential did not exhibit a
163 significant increase with the magnitude of the southward IMF; however, this was not the
164 case when increasing the velocity of the solar wind. Merkine et al. (2003) suggests that the
165 conductivity of the ionosphere is important in determining the scale and saturation of the
166 cross polar cap potential. Our simulation model did not consider ionospheric conductivity
167 and the feedback from the ionosphere to the magnetosphere. Thus, the magnetospheric
168 dynamics corresponding to a strengthening of the southward IMF inhibit the enhancement

169 of the cross polar cap potential.

170

171

172 ## 4. Discussion and conclusions

173

174 The configurations of the magnetic field lines are illustrated in Figs. 3 and 4 to show
175 the effects of the structural change in the dayside magnetic field lines on the cross polar cap
176 potential. The white lines in both figures represent the magnetic field lines, and the magnitude
177 of the magnetic field in the dayside meridian plane is represented using the color spectrum.
178 The magnetic field lines are drawn from the equally interval points. The closed field lines
179 starts from equator and the open field lines and IMF start from x-line at z = 16 R_E. Fig. 3
180 shows the case when the IMF B_Z is −10 nT and Fig. 4 shows that for −45 nT. Comparing
181 the distance of "A" (which indicates the reconnection point) in these figures, the reconnection
182 point comes closer to Earth as the magnitude of the southward IMF increases (9.1 R_E for -10
183 nT and 7.8 R_E for -45 nT). In addition, the Alfvén Mach number (M_A) becomes small then
184 the magnetopauses are flattened in the Z direction (focus on the deep blue region in Figs. 3
185 and 4), which prevents reconnection from occurring at the subsolar point. When the IMF

becomes stronger, M_A becomes smaller so that the magnetosheath region broadens and more magnetic flux lines can exist there. From Fig. 4, it appears that the region with a weak magnetic field (blue colored region in the figure) is not smoothly connected to the cusp. In other words, the strength of the magnetic field, which flows tailward after reconnection on the dayside, suddenly approaches the IMF magnitude around the cusp. To focus on the behavior of reconnected field lines in Figs. 3 and 4, the reconnected field lines are smoothly carried by the solar wind from the subsolar point to the tail for −10 nT case, however those field lines for −45 nT case are not well brought to the tail (see the blue region along the magnetopause in fig. 4). To confirm the effect of solar wind to the transport of reconnected magnetic field, the configurations of the magnetic field lines for the solar wind velocity 600 km s^{-1} with the IMF B_Z -5 nT are illustrated in Fig. 5. The format of Fig. 5 is the same as Figs. 3 and 4. In Fig. 5 the reconnected field lines are well brought smoothly to the tail (focus on the bending magnetic field lines around z-axis). These bending field lines show that reconnected field lines are brought before the magnetic field lines are tightened.

In addition the maximum speed of carrying the reconnected field for -45 nT case is 1.7 times as that for -10 nT case even though the magnitude of southward IMF is different as 4.5 times. These suggest that the reconnected magnetic field does not flow smoothly and

Figure 3
Figure 4
Figure 5

203 stagnates around the subsolar point, and then next reconnection becomes not likely to occur
204 because there is not enough space to merge, causing a decrease in the reconnection rate.
205 Slightly away from the subsolar point, as the magnitude of the southward IMF
206 increases, the velocity of the reconnected flow approaches that of the magnetosheath flow.
207 Thus, if the reconnection jet could connect smoothly to the plasma flow in the magnetosheath,
208 the cross polar cap potential would increase and the reconnection rate would not decrease.
209 That is, there is a relation between the reconnection rate at the subsolar point and the rate at
210 which the magnetic flux lines are drawn away from the reconnection site by the solar wind.
211 The cross polar cap potential is inhibited by that solar wind could not bring the much
212 magnetic flux from dayside to nightside as compared to the reconnected flux. In such a case,
213 the reconnected field lines, whose components are almost southward, remain around the
214 subsolar point and prevent the southward IMF from continually reconnecting with the Earth's
215 magnetic field. This non-reconnected IMF moves to the dawn and dusk sides and flows along
216 the flanks of the magnetopause. The length of the x-line, which indicates broadening of the
217 reconnection region, for variations in the IMF is shown in Fig. 6. The x-line is defined as the
218 line between the open and closed field lines. It is long at low IEF E_Y and short at high E_Y,
219 which also suggests a decrease in the occurrence of reconnection due to the stagnation of

220 reconnected magnetic field lines.

221 In the simulation with increasing IMF magnitudes, the dayside reconnected **Figure 6**
222 magnetic field lines flowed tailward; however, as the velocity of the solar wind was not
223 sufficient (300 km s^{-1}), the reconnected magnetic field lines were not dragged away from
224 around the reconnection region, thereby inhibiting the cross polar cap potential. This
225 prevented the IMF from merging with the Earth's magnetic field on the dayside. Under such
226 conditions, reconnection became difficult, as evidenced by the saturation of RX E_Y. However,
227 in the simulation with increasing solar wind velocities, the reconnected magnetic field lines
228 did not stagnate at the subsolar point and could flow tailward. This was why the cross polar
229 cap potential was not saturated but increased in this case. Considering a kind of criterion for
230 inhibition, it seems that the inhibition start when the M_A becomes 6.1 however it needs more
231 simulation with the combination of solar wind velocity and IMF variations. These results,
232 obtained using the global simulation model, do not disprove the relation between ionospheric
233 conductivity and the cross polar cap potential but indicate a relation between the magnetic-
234 field configuration and the saturated cross polar cap potential, without taking ionospheric
235 effects into consideration.

236

237

238 ## Acknowledgement

239

240 This work was supported by Grant-in-Aid for JSPS Fellows No.09J01416 (K.F.) and a
241 Grant-in-Aid for Creative Scientific Research, “The Basic Study of Space Weather
242 Prediction” (17GS0208, Head Investigator: K. Shibata), from the Ministry of Education,
243 Science, Sports, Technology, and Culture of Japan and CREST, the Japan Science and
244 Technology Agency (JST). Computing support was provided by the Information
245 Technology Center, Nagoya University, and by the National Institute of Information and
246 Communications Technology (NICT).

247

248 ## References

249

250 Fedder, J. A., and J. G. Lyon, The solar wind-magnetosphere-ionosphere current-voltage
251 relationship, Geophys. Res. Lett., 14, 880– 883, 1987.

252

253 Hill, T. W., Magnetic merging in a collisionless plasma, J. Geophys. Res.,80, 4689-4699,

1975.

Hill, T. W., A. J. Dessler, and R. A. Wolf, Mercury and Mars: The role of ionospheric conductivity in the acceleration of magnetospheric particles, Geophys. Res. Lett., 3, 429–432, 1976.

MacDougall, J. W. and Jayachandran, P. T., 2006, Polar cap voltage saturation, J. Geophys. Res., 111, A12306, doi: 10.1029/2006JA011741.

Merkine, V. G., Papadopoulos, K., Milikh, G., Sharma, A. S., Shao, X., Lyon, J., and Goodrich, C., 2003, Effects of the solar wind electric field and ionospheric conductance on the cross polar cap potential: Results of global MHD modeling, Geophys. Res. Lett., 30, 2180, doi: 10.1029/2003GL017903.

Nagatsuma, T., Saturation of polar cap potential by intense solar wind electric field. Geophys. Res. Lett., 29, 10.1029/2001GL014202, 2002.

271 Ogino, T., 1986, A three-dimensional MHD simulation of the interaction of the solar wind
272 with the Earth's magnetosphere: The generation of field-aligned currents, J. Geophys. Res.,
273 91, 6791-6806.
274
275 Ogino, T., Walker, R. J., and Ashour-Abdalla, M., 1992, A global magnetohydrodynamic
276 simulation of the magnetosheath and magnetosphere when the interplanetary magnetic field
277 is northward, IEEE Trans. Plasma Sci., 20, 817-828.
278
279 Park, K. S., Ogino, T., and Walker, R. J., 2006, On the importance of antiparallel
280 reconnection when the dipole tilt and IMF B_Y are nonzero, J. Geophys. Res., 111, A05202,
281 doi: 10.1029/2004JA010972.
282
283 Raeder, J. and Lu, G., 2005, Polar cap potential saturation during large geomagnetic storms,
284 Adv. Space Res., 36, 1804-1808.
285
286 Ridley, A. J., 2005, A new formulation for the ionospheric cross polar cap potential
287 including saturation effects, Ann. Geophys., 23, 3533-3547.

288

289 Russell, C.T., Luhmann, J. G., Lu, G., 2001, Nonlinear response of the polar ionosphere to
290 large values of the interplanetary electric field, J. Geophys. Res., 106, 18495-18504.

291

292 Siscoe, G. L., Crooker, N. U., and Siebert, K. D., 2002, Transpolar potential saturation:
293 Roles of region 1 current system and solar wind ram pressure, J. Geophys. Res., 107, 1321,
294 doi:10.1029/2001JA009176.

295

296 Siscoe, G., Raeder, J., and Ridley, A. J., 2004, Transpolar potential saturation models
297 compared, J. Geophys. Res., 109, A09203, doi: 10.1029/2003JA010318.

298

299 Sonnerup, B. U. O., Magnetopause reconnection rate, J. Geophys. Res., 79, 1546- 1549,
300 1974.

301

302 Walker, R. J., Ogino, T., Raeder, J., and Ashour-Abdalla, M., 1993, A global
303 magnetohydrodynamic simulation of the magnetosphere when the interplanetary magnetic
304 field is southward: The onset of magnetotail reconnection, J. Geophys. Res., 98, 17235-
305 17249.

306

307 Weimer, D. R., L. A. Reinleitner, J. R. Kan, L. Zhu, and S.-I. Akasofu, Saturation of the

308 auroral electrojet current and the polar cap potential, J. Geophys. Res., 95, 18,981–18,987,

309 1990.

310

311

312 **FIGURES**

313

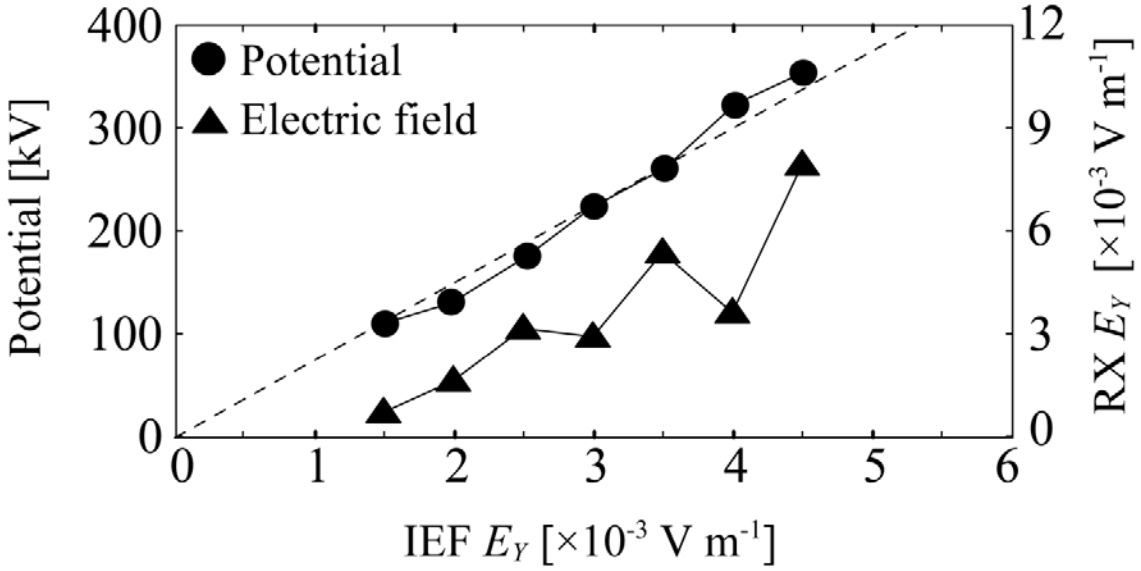

314

315 Fig. 1. Dependence of interplanetary electric field (IEF) on cross polar cap potential and

316 electric field of dayside reconnection (RX) for solar wind velocities listed in Table 1.

317 Horizontal axis represents Y-component of IEF, and left vertical axis, the potential. Right

318 vertical axis represents Y-component of RX. Black circles represent potential and triangles,

319 electric field.

320

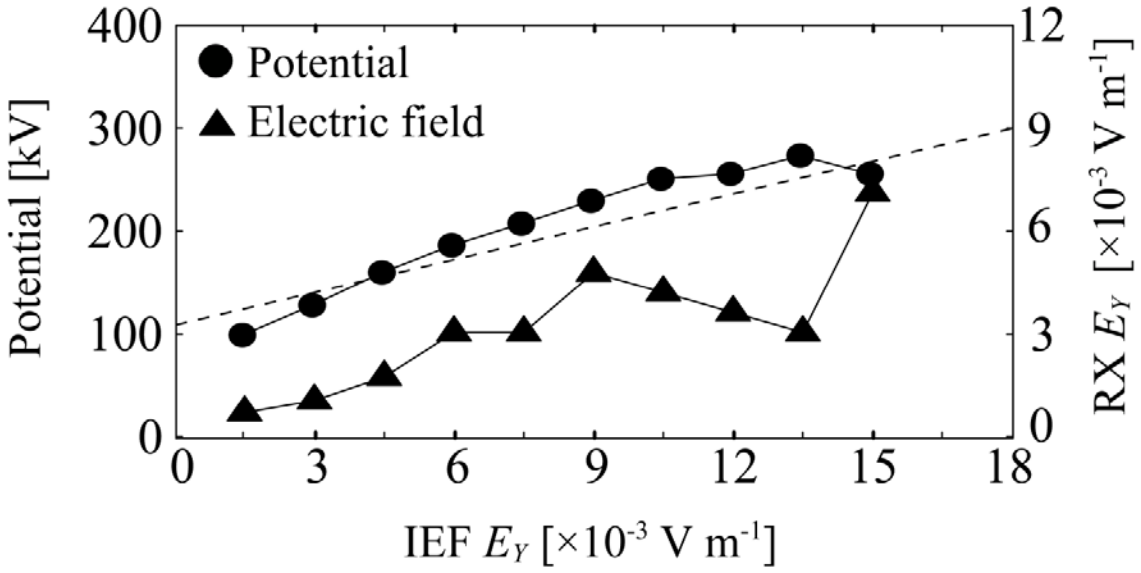

321

322 Fig. 2. Dependence of interplanetary electric field (IEF) on cross polar cap potential and

323 electric field of dayside reconnection (RX) for IMF magnitudes listed in Table 2. Legend is

324 same as that of Fig. 1.

325

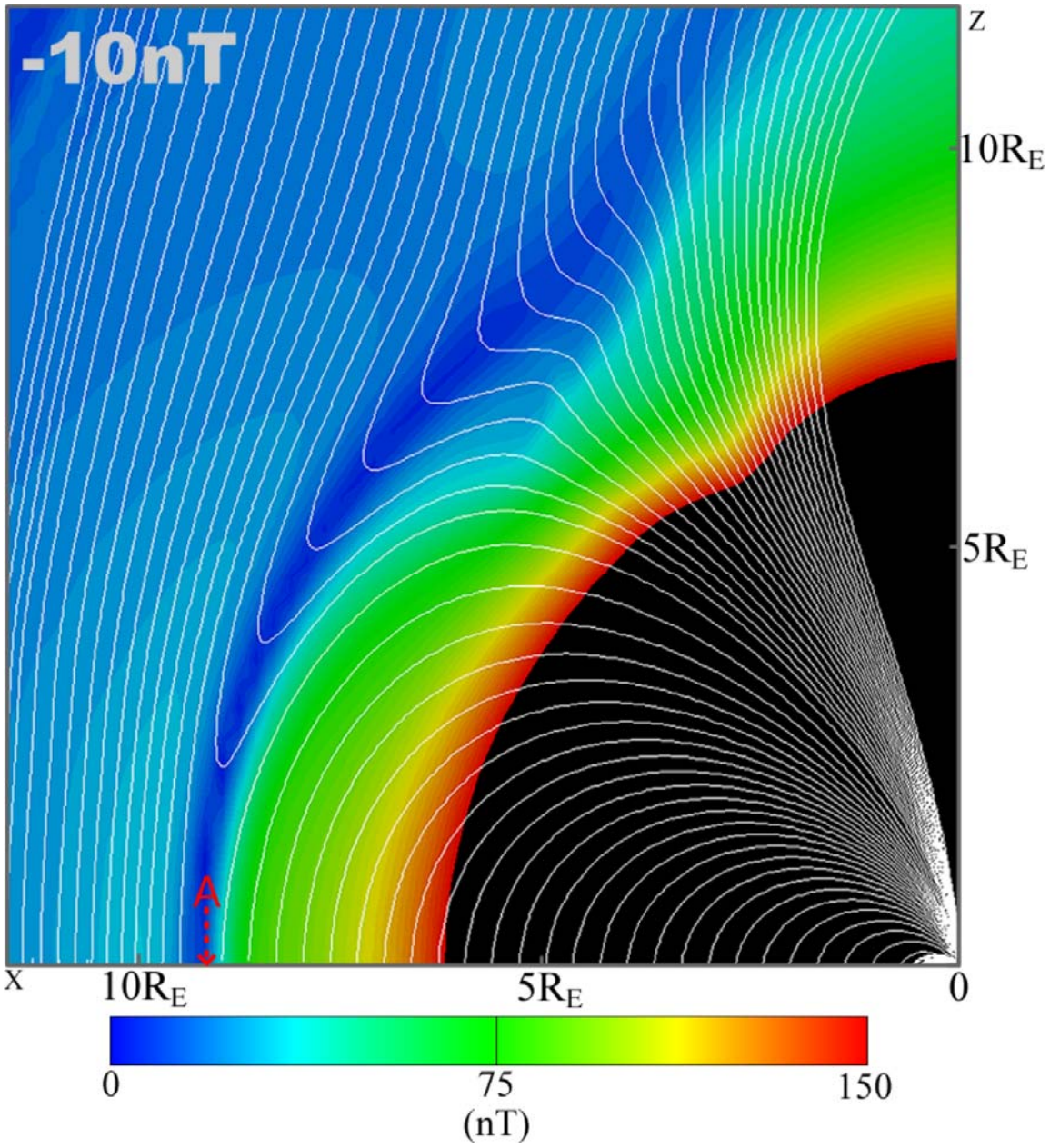

Fig. 3. Configuration and magnitude of magnetic field lines in dayside meridian plane for IMF B_Z of −10 nT. White lines indicate magnetic field lines and color spectrum represents magnitude. "A" indicates the reconnection point (9.1 R_E) on the Sun-Earth line.

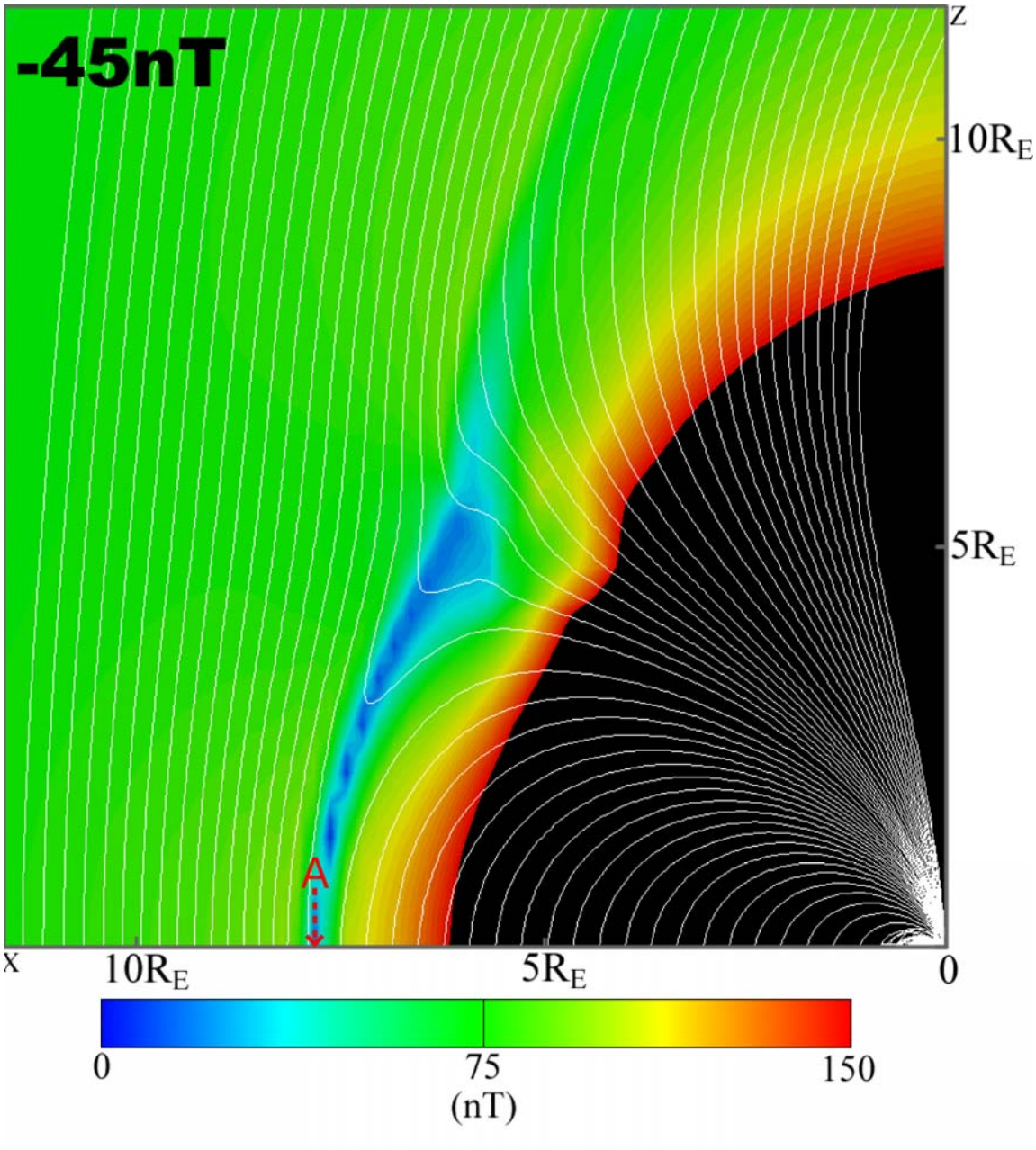

330

331 Fig. 4. Configuration and magnitude of magnetic field lines in dayside meridian plane for

332 IMF B_Z of −45 nT. White lines indicate magnetic field lines and color spectrum represents

333 magnitude. “A” indicates the reconnection point (7.8 R_E) on the Sun-Earth line.

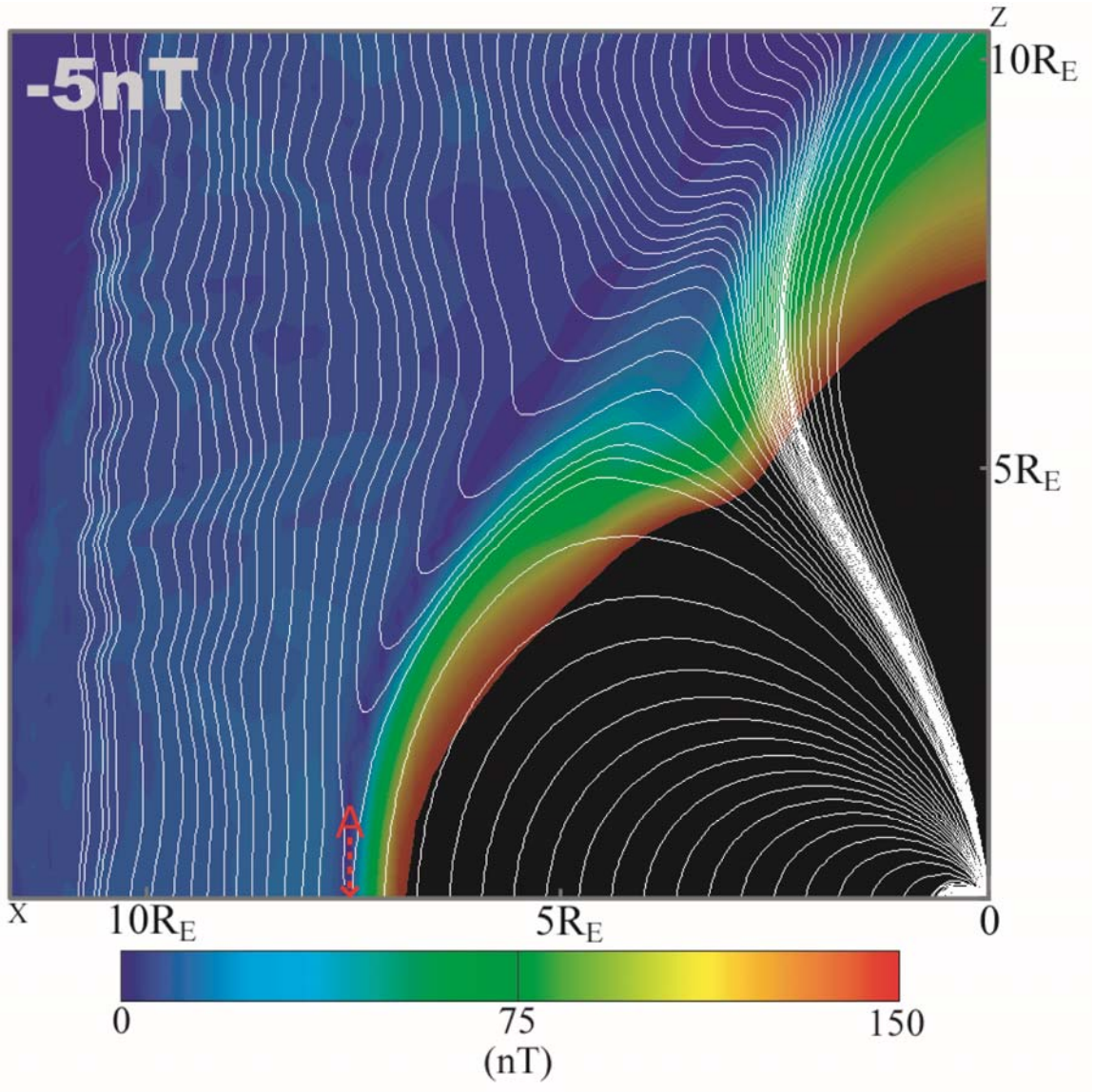

Fig. 5. Configuration and magnitude of magnetic field lines in dayside meridian plane for IMF B_Z of −5 nT with 600km/s solar wind. White lines indicate magnetic field lines and color spectrum represents magnitude. “A” indicates the reconnection point (7.5 R_E) on the Sun-Earth line.

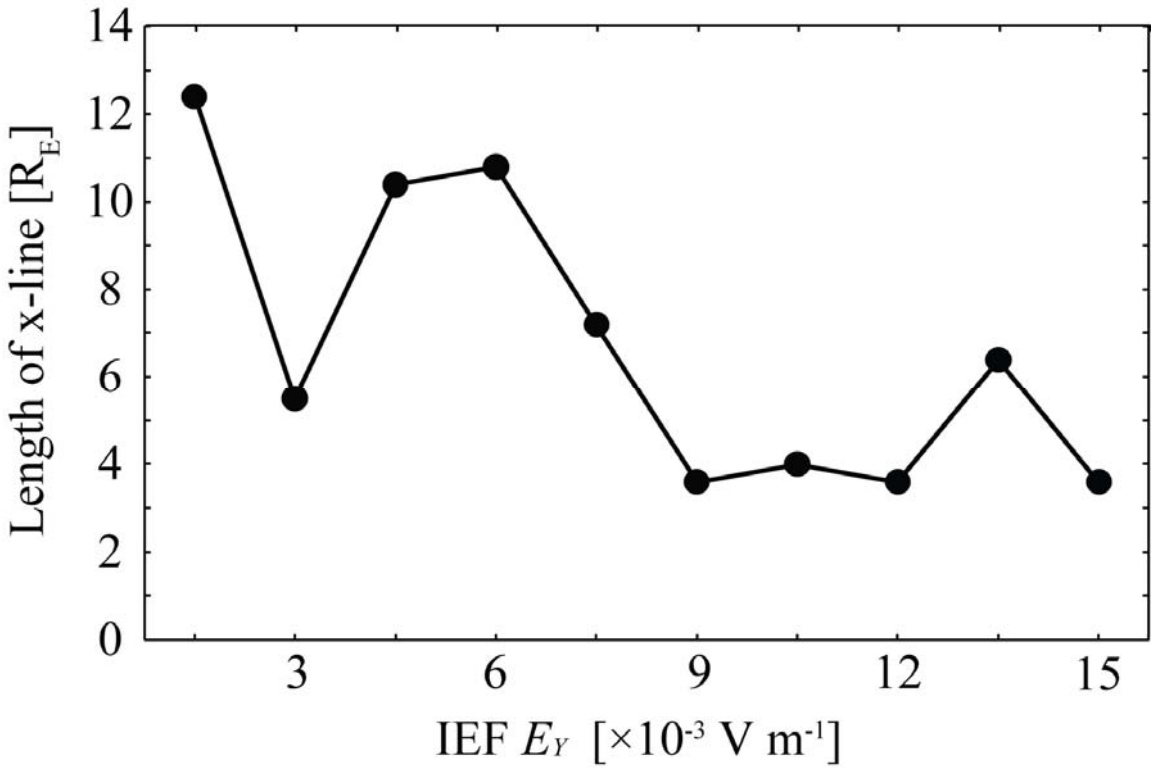

Fig. 6. Dependence of interplanetary electric field (IEF) on length of x-line on dayside for IMF magnitudes listed in Table 2. Horizontal axis represents Y-component of IEF and vertical axis, length of x-line.

TABLES

Table 1. Velocity of solar wind, Y-component of IEF (E_Y), and Alfvén Mach number (M_A) used in simulation (IMF B_Z is set to −5 nT).

348

349 Table 2. Z-component of IMF (B_Z), Y-component of IEF (E_Y), and Alfvén Mach number

350 (M_A) used in simulation (velocity of solar wind is 300 km s^{-1}).

351